Theoretical study on electronic and optical properties of mixed valence perovskite $Cs_2Au_2X_6$ (X=Cl, Br, I)

Shugo Suzuki and Makoto Tsuyama

Division of Materials Science, Faculty of Pure and Applied Sciences, University of Tsukuba, Tsukuba, Ibaraki 305-8573, Japan

We study the electronic and optical properties of the mixed valence perovskite $Cs_2Au_2X_6$ (X=Cl, Br, I) using the fully relativistic all-electron calculations. We find that $Cs_2Au_2X_6$ exhibit indirect fundamental band gaps although the differences between the indirect and direct band gaps are small. For the electric field of light perpendicular to the tetragonal c axis, $Cs_2Au_2Br_6$ and $Cs_2Au_2I_6$ exhibit the maximum absorption coefficient of about 20 $\times 10^4$ cm^{-1} around the photon energy of 2 eV, which is considerably larger than that of $CH_3NH_3PbI_3$. For the electric field of light parallel to the tetragonal c axis, the absorption coefficient of $Cs_2Au_2I_6$ is comparable to that of $CH_3NH_3PbI_3$ in the main part of the solar spectrum. Furthermore, we estimate the photovoltaic performance of $Cs_2Au_2X_6$ employing the spectroscopically limited maximum efficiency as a metric and discuss its dependence on the film thicknes in detail.

1. Introduction

During the last decade, organic-inorganic lead halide perovskite $MAPbI_3$ (MA = CH_3NH_3) has been extensively studied as a promising material for photovoltaic applications due to its low manufacturing cost based on simple solution process and high power conversion efficiency (PCE).[1–8] The outstanding performance of $MAPbI_3$ as an absorber material is originated from its excellent electrical and optical properties: high and balanced electron and hole mobilities, high absorption coefficients, long carrier lifetimes and diffusion lengths, and band-gap tunability.

However, two main challenges that need to be addressed still remain. $MAPbI_3$ tends to degrade when exposed to air, heat, or humidity.[9] At the same time, the toxicity of lead is still an unsolved problem.[10,11] Many studies have been carried out to find lead-free perovskite materials by substituting lead with other non-toxic elements.[12–26] One way is through homovalent substitution of lead with another divalent element in the perovskite structure.[13–19] Another way is heterovalent substitution, as first proposed by Giorgi and Yamashita,[20] introducing a double perovskite structure with chemical formula $A_2BB'X_6$, where A is an A-site cation and X is a halogen ion while B and B' represent monovalent and trivalent B-site cations,

respectively.[20–26)]

Recently, Debbichi et al. proposed that mixed valence perovskite $Cs_2Au_2I_6$, which can be viewed as a material with a distorted double perovskite structure with both B and B' being Au, is a potential lead-free material with ultrahigh PCE.[27)] They reported that the calculated absorption coefficient of $Cs_2Au_2I_6$ is very high, almost 70 $\times 10^4$ cm^{-1} around the photon energy of 2 eV. Subsequently, Giorgi et al. studied $Cs_2Au_2I_6$ using a combined fully ab initio approach based on density functional and many-body perturbation theories and showed that the exciton in this material is weakly bounded as in $MAPbI_3$.[28)] Furthermore, very recently, Kangsabanik et al. theoretically studied the electronic and optical properties of $Cs_2Au_2X_6$ (X=Cl, Br, I) and concluded that $Cs_2Au_2I_6$ exhibits higher PCE than $MAPbI_3$.[29)]

However, there exist discrepancies between the results reported by the previous theoretical studies. One discrepancy is that the fundamental band gap reported by Debbichi et al. is direct while that reported by Kangsabanik et al. is indirect although the difference between the direct and indirect band gaps is small. Another discrepancy is regarding the magnitude of the calculated absorption coefficients; the absorption coefficient calculated by Debbichi et al. is an order of magnitude larger than that calculated by Kangsabanik et al. Since the dependence of the PCE on film thickness is very sensitive to the magnitude of the absorption coefficient, a difference of an order of magnitude can affect it drastically. In view of this, further theoretical and experimental studies are needed on the electronic and optical properties as well as the PCE of $Cs_2Au_2X_6$.

The purpose of this work is to study the electronic and optical properties of the mixed valence perovskite $Cs_2Au_2X_6$ (X=Cl, Br, I) using the fully relativistic all-electron calculations based on the density functional theory. In particular, we calculate the absorption coefficients using the four-component spinors obtained as the solutions of the Dirac-Kohn-Sham equations. Using the calculated absorption coefficients, we estimate the PCE of the materials based on a metric for quantifying the photovoltaic performance. We compare the calculated absorption coefficients and the estimated PCE of $Cs_2Au_2X_6$ with those of $MAPbI_3$. The method of calculations is explained in Sect. 2. The results and discussion are given in Sect. 3. Finally, we give the conclusions of this work in Sect. 4.

2. Method of calculations

The ternary compound $Cs_2Au_2X_6$ (X=Cl, Br, I) is a mixed valence gold complex with a distorted perovskite structure.[30–35)] $Cs_2Au_2X_6$ crystallizes in a tetragonal structure with space group I4/mmm as shown in Fig. 1, which was depicted using VESTA.[36)] The crystal structure

consists of a metal-halogen framework formed by two types of AuX_6 octahedra; one is compressed AuX_6 octahedra and the other is elongated AuX_6 octahedra. The compressed and elongated AuX_6 octahedra are three-dimensionally and alternately arranged along the [001] and [110] directions, sharing the X atom at each corner of the octahedra and forming a rocksalt-like structure. The structure is also characterized by the assembly of the linear AuX_2^- and square AuX_4^- complex ions arranged alternately accompanied with charge disproportionation. The Au atoms in the compressed AuX_6 octahedra or the linear AuX_2^- complex ions are in the monovalent state, Au^{I}, while those in the elongated AuX_6 octahedra or the square AuX_4^- complex ions are in the trivalent state, Au^{III}.

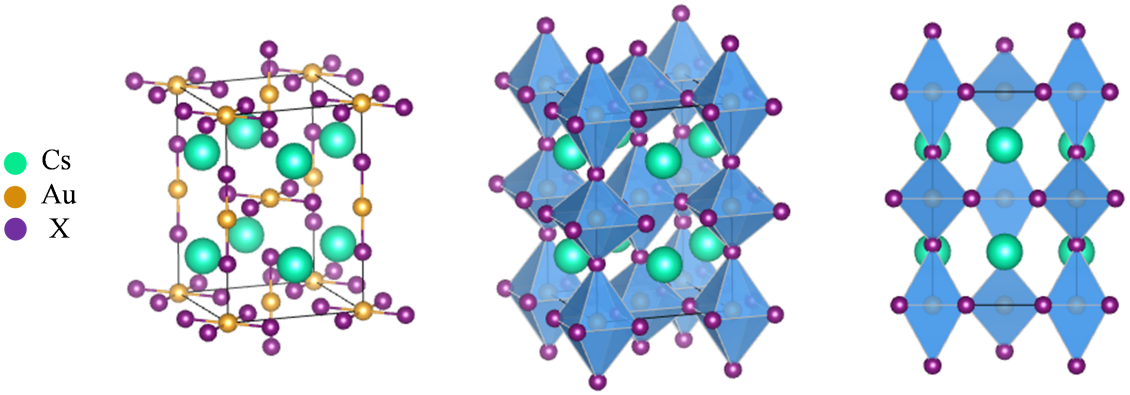

Fig. 1. Schematic diagram of the structure of $Cs_2Au_2X_6$. The structure consists of a metal-halogen framework formed by compressed and elongated AuX_6 octahedra arranged alternately along the [001] and [110] directions, sharing the X atom at each corner of the octahedra and forming a rocksalt-like structure. The structure is also characterized by the assembly of the linear AuX_2^- and square AuX_4^- complex ions arranged alternately.

We carried out all-electron calculations based on the density functional theory.[37–41] The generalized gradient approximation (GGA) to the exchange-correlation energy functional was adopted using the Perdew-Burke-Ernzerhof form.[42] The lattice constants and the atomic positions were optimized with the scalar relativistic full-potential linear-combination-of-atomic-orbitals method.[39] Using the optimized structures, the band structures, the densities of states, and the absorption coefficients were calculated with the fully relativistic full-potential linear-combination-of-atomic-orbitals method.[38,40]

The absorption coefficients were obtained from the optical conductivity calculated within the independent particle approximation combined with a phenomenological approach.[40,41] The optical transition matrix elements were calculated using the four-component spinors

obtained as the solutions of the Dirac-Kohn-Sham equations to take into account all the relativistic effects including spin-orbit coupling. Also, the phenomenological relaxation-time parameter $\hbar/\tau$ was used to simulate the lifetime of excitations; for all the materials studied in this work $\hbar/\tau = 0.3$ eV was used.

Using the calculated absorption coefficients, we evaluated the PCE employing the spectroscopically limited maximum efficiency (SLME) as a metric for quantifying the photovoltaic performance.[43] The SLME is a generalization of the Shockley-Queisser (SQ) limit.[44] One important feature of the SLME is that for a material whose fundamental band gap is indirect, the SLME takes into account the non-radiative recombination by considering $\Delta = E_{\mathrm{g}}^{\mathrm{da}} - E_{\mathrm{g}}$, where E_{g} and $E_{\mathrm{g}}^{\mathrm{da}}$ are the fundamental and direct allowed band gaps, respectively. Also, another important point is that the SLME considers the material dependent absorption coefficient in the expression $a(E) = 1 - e^{-2\alpha(E)L}$, where $a(E)$, $\alpha(E)$, and L are the absorptivity, the absorption coefficient, and the film thickness, respectively. Note that the SLME is very sensitive to $\alpha(E)$ because $a(E)$ depends exponentially on $\alpha(E)$. In calculating the SLME, the standard AM1.5G solar spectrum is used.[45]

The atomic orbitals used as the basis functions are as follows: the $1s$, $2s$, $2p$, $3s$, $3p$, $3d$, $4s$, $4p$, $4d$, $5s$, $5p$, $6s$ orbitals of the neutral Cs atom; the $6s$, $6p$ orbitals of the Cs^{2+} atom; the $5d$ orbitals of the Cs^{6+} atom; the $1s$, $2s$, $2p$, $3s$, $3p$, $3d$, $4s$, $4p$, $4d$, $4f$, $5s$, $5p$, $5d$, $6s$ orbitals of the neutral Au atom; the $6s$, $6p$ orbitals of the Au^{2+} atom; the $5d$ orbitals of the Au^{6+} atom; the $1s$, $2s$, $2p$, $3s$, $3p$, orbitals of the neutral Cl atom; the $3s$, $3p$, $3d$ orbitals of the Cl^{2+} atom; the $1s$, $2s$, $2p$, $3s$, $3p$, $3d$, $4s$, $4p$ orbitals of the neutral Br atom; the $4s$, $4p$, $4d$ orbitals of the Br^{2+} atom; the $1s$, $2s$, $2p$, $3s$, $3p$, $3d$, $4s$, $4p$, $4d$, $5s$, $5p$ orbitals of the neutral I atom; the $5s$, $5p$, $5d$ orbitals of the I^{2+} atom. It is worth noting that using the atomic orbitals of positively charged atoms as well as those of neutral atoms is crucial to describing the contraction of atomic orbitals associated with cohesion. The Brillouin zone sampling for the structure optimization was performed using a $4\times4\times4$ $\boldsymbol{k}$ point grid. We used the force criterion of 0.01 eV/Å to stop the optimization of the atomic positions. We used 185 $\boldsymbol{k}$ points generated with the good-lattice-point method for calculating the self-consistent potential.[46] We used 418 $\boldsymbol{k}$ points generated with the good-lattice-point method for calculating the absorption coefficients. The band structures were calculated along the path connecting the symmetry points in the Brillouin zone given by Setyawan and Curtarolo.[47]

3. Results and discussion

In Table I, the calculated and experimental lattice constants are shown. The deviation from the experimental values is about +2% for a and +4% for c. Also, in Table II, the calculated and experimental Au-X bond lengths are shown. Since $Cs_2Au_2X_6$ consist of alternating compressed and elongated AuX_6 octahedra, there exist two kinds of Au-X bonds; one is the shorter apical Au^{I}-X bonds in the linear AuX_2^- complex ions and the other is the longer equatorial Au^{III}-X bonds in the square AuX_4^- complex ions. The deviation from the experimental values is about +6%.

Table I. Calculated and experimental lattice constants of $Cs_2Au_2X_6$ (in Å).

Material	a		c	
	Calc.	Expt.	Calc.	Expt.
$Cs_2Au_2Cl_6$	7.61	7.50[a)]	11.33	10.88[a)]
$Cs_2Au_2Br_6$	7.96	7.79[b)]	11.85	11.38[b)]
$Cs_2Au_2I_6$	8.51	8.28[c)]	12.59	12.09[c)]

a) Ref. 31.
b) Ref. 32.
c) Ref. 33.

Table II. Calculated and experimental Au-X bond lengths (in Å) in $Cs_2Au_2X_6$. The apical Au^{I}-X bond lengths for the linear AuX_2^- complex ions and the equatorial Au^{III}-X bond lengths for the square AuX_4^- complex ions are shown.

Material	Au^{I}-X		Au^{III}-X	
	Calc.	Expt.	Calc.	Expt.
$Cs_2Au_2Cl_6$	2.41	2.28[a)]	2.45	2.29[a)]
$Cs_2Au_2Br_6$	2.54	2.41[b)]	2.58	2.45[b)]
$Cs_2Au_2I_6$	2.72	2.59[c)]	2.78	2.65[c)]

a) Ref. 31.
b) Ref. 32.
c) Ref. 33.

In Fig. 2, the calculated band structures and the densities of states of $Cs_2Au_2X_6$ are shown. It is found that the fundamental band gaps of $Cs_2Au_2X_6$ are all indirect: E_g = 0.28, 0.35, and 0.39 eV for X=Cl, Br, and I, respectively. The conduction band minimum and the valence band

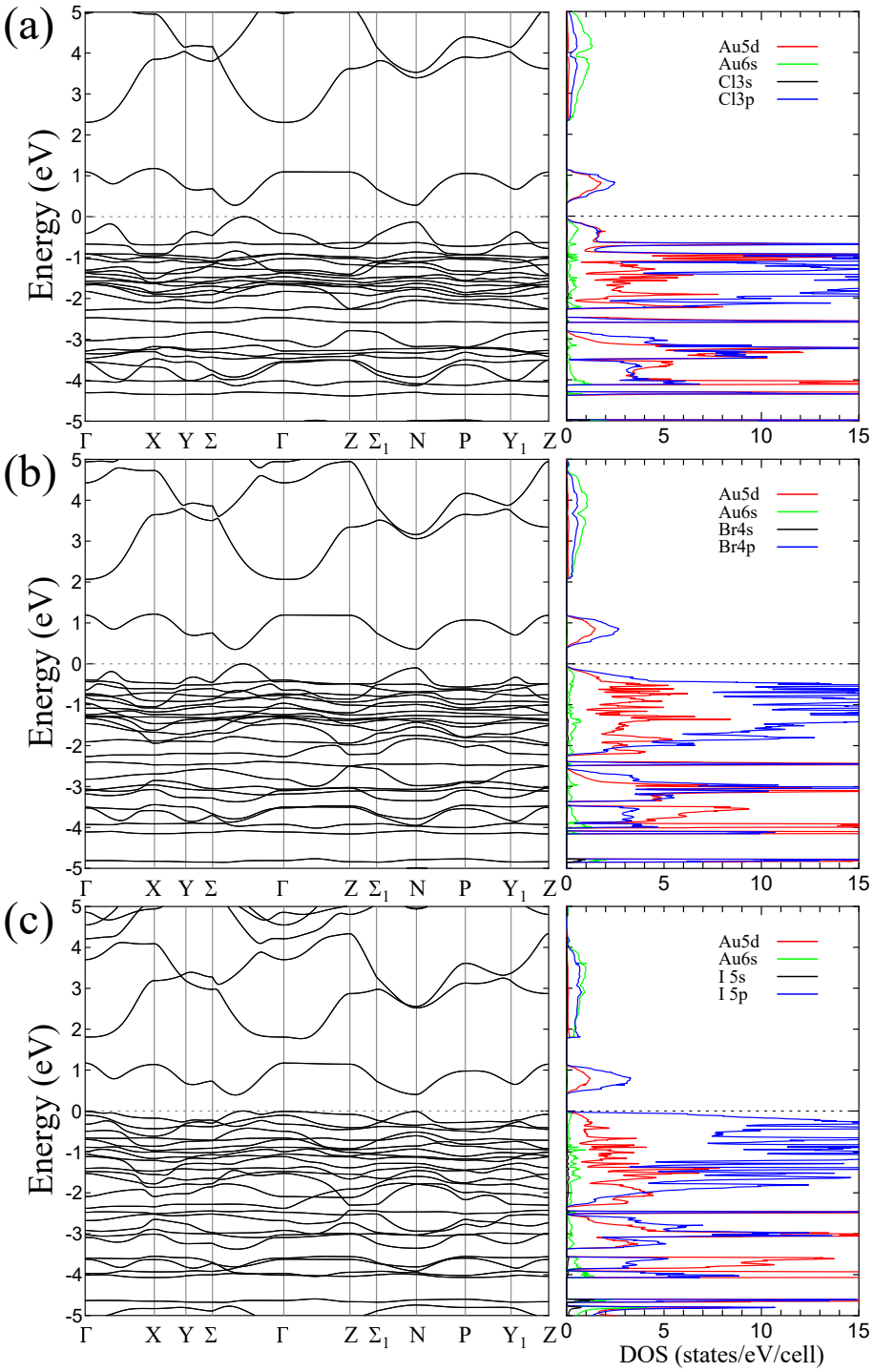

Fig. 2. Band structures and densities of states of (a) $Cs_2Au_2Cl_6$, (b) $Cs_2Au_2Br_6$, and (c) $Cs_2Au_2I_6$. The zero of the energy is taken at the top of the valence bands.

maximum are located at two distinct points between Σ and Γ. The conduction and valence bands are both mainly composed of the Au 5*d* and *X* *np* orbitals, where *n*=3, 4, and 5 for *X*=Cl, Br, and I, respectively. The direct band gaps of $Cs_2Au_2X_6$ are at the N point: E_g^{da} =

0.41, 0.46, and 0.42 eV for X=Cl, Br, and I, respectively. The differences between the indirect and direct band gaps, Δ, are 0.13, 0.11, and 0.03 eV, for X=Cl, Br, and I, respectively. Note that Δ are small. In particular, Δ for $Cs_2Au_2I_6$ is only 0.03 eV. Accordingly, a subtle difference in the calculations, e.g., differences in the lattice constants and the atomic positions, can affect whether the fundamental band gaps are indirect or direct. In fact, Debbichi et al. reported that $Cs_2Au_2I_6$ exhibits a direct band gap while Kangsabanik et al. reported that it exhibits an indirect band gap.[27,29)]

Since our calculated band gaps, 0.28, 0.35, and 0.39 eV for X=Cl, Br, and I, respectively, are obtained using GGA, they are underestimated in comparison with the experimental band gaps. The experimental band gaps of $Cs_2Au_2X_6$ are 2.04, 1.60, and 1.31 eV for X=Cl, Br, and I, respectively.[34)] Thus, the underestimation due to GGA is 1.76, 1.25, and 0.92 eV for X=Cl, Br, and I, respectively. The amount of underestimation decreases with changing X from Cl to Br to I. This trend may be understood considering the fact that the self-interaction correction of the X np electron is smaller for heavier X because the X np orbital is more delocalized for heavier X. The previous theoretical studies calculated the band gap of $Cs_2Au_2X_6$ using methods beyond GGA.[27–29)] Debbichi et al. reported that the band gap of $Cs_2Au_2I_6$ calculated using a hybrid exchange-correlation energy functional is 1.21 eV. Giorgi et al. also reported that the band gap of $Cs_2Au_2I_6$ calculated using the GW method is 1.35 eV.[27,28)] Furthermore, Kangsabanik et al. reported that the band gaps of $Cs_2Au_2X_6$ calculated using a hybrid exchange-correlation energy functional is 2.08, 1.61, and 1.45 eV for X=Cl, Br, and I, respectively.[29)]

We next show the calculated absorption spectra of $Cs_2Au_2X_6$ in Fig. 3. The absorption spectrum of $MAPbI_3$ calculated in our previous work is also shown in Fig. 3 for comparison.[41)] Since the crystal structure of $Cs_2Au_2X_6$ is tetragonal, the absorption coefficients for the electric field of light perpendicular to the c axis, $E \perp c$, and those for the electric field of light parallel to the c axis, $E \parallel c$, are different. We show the absorption coefficients for $E \perp c$ in Fig. 3(a) and those for $E \parallel c$ in Fig. 3(b). For each of the calculated absorption spectra, the scissors correction is applied to correct the underestimation of the GGA band gaps using the experimental band gaps mentioned above: 2.04, 1.60, and 1.31 eV for X=Cl, Br, and I, respectively.[34)] We also used the experimental band gap of 1.61 eV for $MAPbI_3$.[48)] Since we are interested in the energy region of the main part of the solar spectrum, i.e., 1 to 3 eV, we will focus on the absorption spectra in this energy region in the following.

The absorption edges for X=Cl, Br, and I are located at about 2.0, 1.6, and 1.3 eV, respectively, in accordance with the scissors correction. For $E \perp c$, the absorption coefficients of $Cs_2Au_2Br_6$ and $Cs_2Au_2I_6$ are considerably larger than that of $MAPbI_3$; the absorption

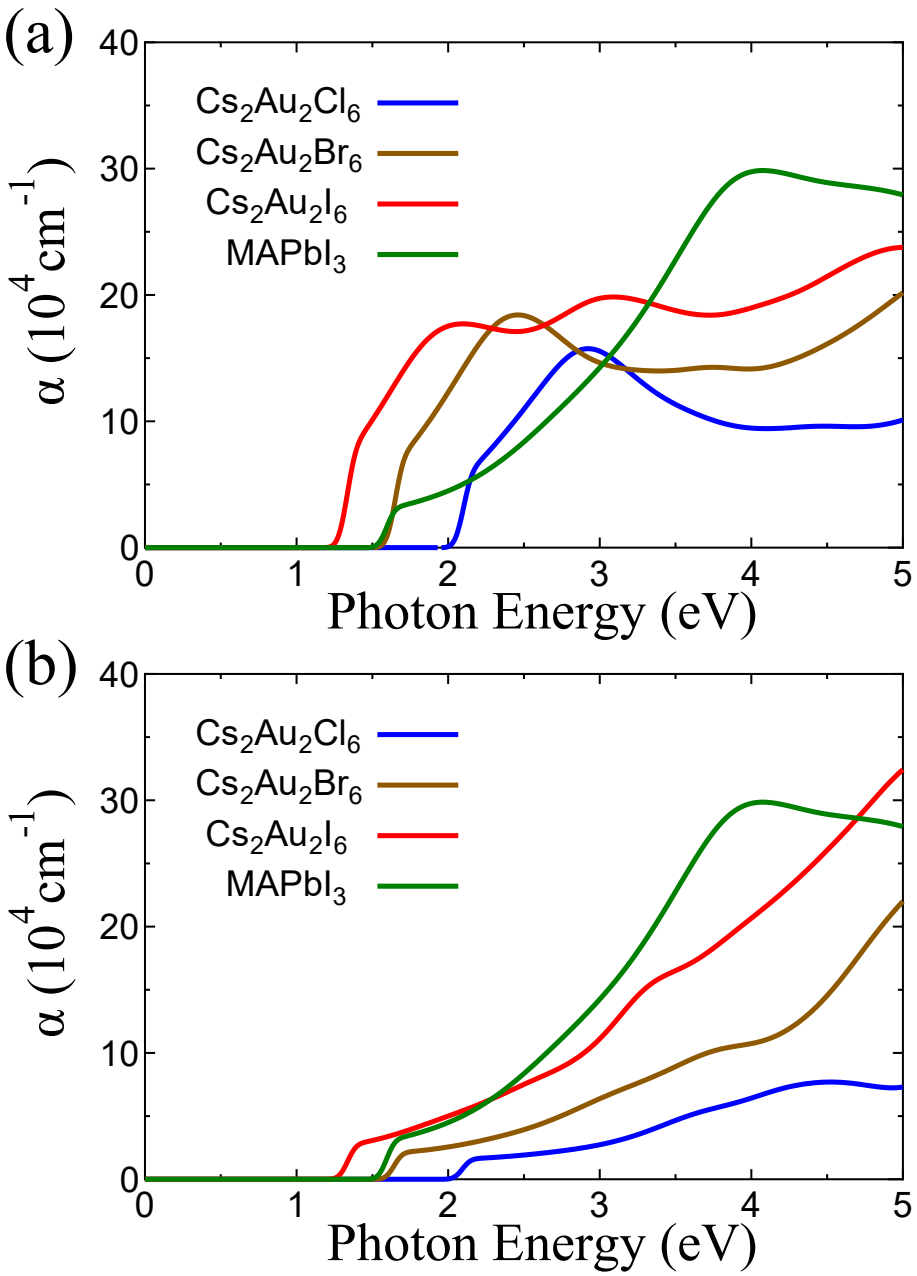

Fig. 3. Calculated absorption coefficients α of $Cs_2Au_2Cl_6$, $Cs_2Au_2Br_6$, $Cs_2Au_2I_6$, and $MAPbI_3$ for the electric field of light (a) perpendicular and (b) parallel to the c axis. All the calculated absorption spectra are scissors corrected.

coefficients of $Cs_2Au_2Br_6$ and $Cs_2Au_2I_6$ reach almost 20 $\times 10^4$ cm^{-1} around 2 eV. On the contrary, the absorption of $Cs_2Au_2Cl_6$ is absent below 2 eV due to its relatively large band gap although its absorption coefficient is comparable to that of $MAPbI_3$ in the high-energy part of the solar spectrum, 2 to 3 eV. For $E \parallel c$, the absorption coefficient of $Cs_2Au_2I_6$ is

comparable to that of $MAPbI_3$. On the other hand, the absorption coefficients of $Cs_2Au_2Cl_6$ and $Cs_2Au_2Br_6$ are small in comparison with those of $Cs_2Au_2I_6$ and $MAPbI_3$.

As mentioned above, the absorption coefficient of $Cs_2Au_2I_6$ is considerably larger than that of $MAPbI_3$. This is in agreement with the results reported by Debbichi et al.[27] However, the maximum value of their calculated absorption coefficient of $Cs_2Au_2I_6$ for $E \perp c$ reaches almost 70 $\times 10^4$ cm^{-1} around 2 eV, which is three to four times larger than our calculated maximum absorption coefficient of about 20 $\times 10^4$ cm^{-1}. Furthermore, the calculated absorption coefficient of $Cs_2Au_2I_6$ for $E \perp c$ around 2 eV reported by Kangsabanik et al. is 6 $\times 10^4$ cm^{-1}, which is an order of magnitude smaller than that reported by Debbichi et al. and one-third to one-fourth of the maximum absorption coefficient obtained in this work. Although the origin of the discrepancy is not clear, further theoretical and experimental studies are needed.

In Fig. 4, we show the SLME calculated for $Cs_2Au_2X_6$. We also show the SLME calculated for $MAPbI_3$ for comparison. The SLME is obtained using the calculated absorption coefficients and the differences between the indirect and direct band gaps, Δ, which is 0.13, 0.11, and 0.03 eV, for X=Cl, Br, and I, respectively, while zero for $MAPbI_3$. For both $E \perp c$ and $E \parallel c$, the SLME in the limit of large film thickness is 20%, 28%, and 31% for X=Cl, Br, and I, respectively. These values are close to the SQ limit, 22%, 30%, and 33% for X=Cl, Br, and I, respectively. The reason why each of the SLME in the limit of large film thickness is slightly smaller than the corresponding SQ limit is the small but non-zero Δ. On the other hand, for $MAPbI_3$, the SLME in the limit of large film thickness, 31%, coincides with its SQ limit because its Δ is zero. The SLME of $Cs_2Au_2I_6$ in the limit of large film thickness, 31%, is almost the same as that of $MAPbI_3$. This is due to the fact that Δ of $Cs_2Au_2I_6$, 0.03 eV, is considerably small and its band gap, 1.31 eV, is nearly optimal for the high SQ limit. The SLME of $Cs_2Au_2Br_6$ in the limit of large film thickness, 28%, is somewhat lower than those of $Cs_2Au_2I_6$ and $MAPbI_3$ although its band gap is almost the same as that of $MAPbI_3$. This is due to the relatively large value of Δ of $Cs_2Au_2Br_6$, 0.11 eV. The SLME of $Cs_2Au_2Cl_6$ in the limit of large film thickness, 20%, is much lower than those of the other materials due to its larger band gap, 2.04 eV, and larger Δ, 0.13 eV.

As shown in Fig. 4(a), the SLME of $Cs_2Au_2Br_6$ and $Cs_2Au_2I_6$ for $E \perp c$ almost reach the large film thickness limit at the film thickness of about 200 nm because of their large absorption coefficients. In particular, the SLME of $Cs_2Au_2I_6$ reaches 98% of its large film thickness limit at the film thickness of 200 nm. Also, at any given film thickness, the SLME of $Cs_2Au_2I_6$ is always larger than that of $MAPbI_3$. It is also worth noting that the SLME of $Cs_2Au_2Br_6$ is larger than that of $MAPbI_3$ for the film thicknesses less than 200 nm. On the

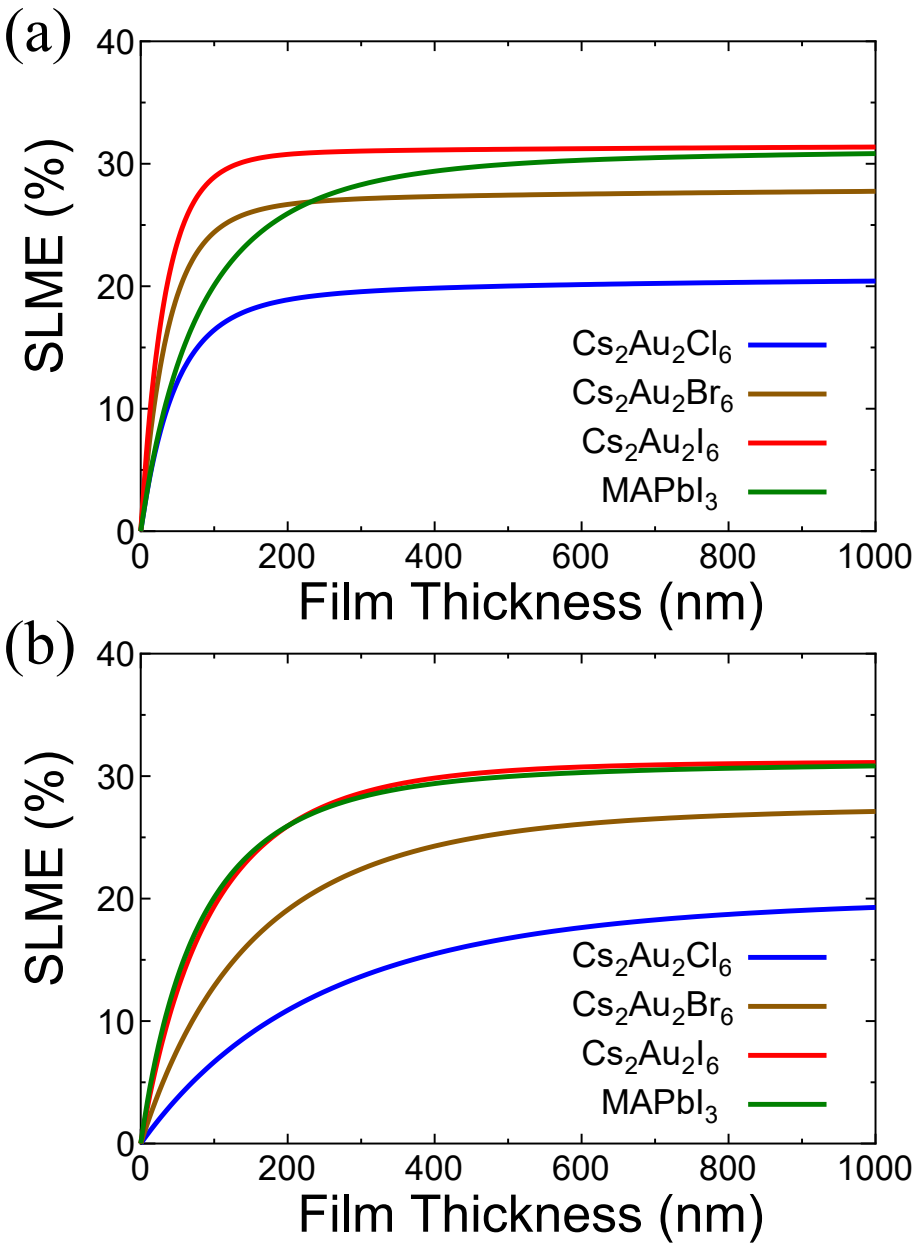

Fig. 4. Calculated SLME of $Cs_2Au_2Cl_6$, $Cs_2Au_2Br_6$, $Cs_2Au_2I_6$, and $MAPbI_3$ as a function of film thickness for the electric field of light (a) perpendicular and (b) parallel to the c axis.

other hand, the SLME of $Cs_2Au_2Cl_6$ is always less than those of the other materials. As shown in Fig. 4(b), the SLME of $Cs_2Au_2I_6$ for $E \parallel c$ is almost equal to that of $MAPbI_3$ at any given film thickness. On the other hand, the SLME for $Cs_2Au_2Cl_6$ and $Cs_2Au_2Br_6$ are smaller than those of $Cs_2Au_2I_6$ and $MAPbI_3$.

The SLME of $Cs_2Au_2X_6$ was also studied by Kangsabanik et al.[29] The most notable

difference from our results is the film thickness dependence of the SLME. Because of the small absorption coefficient calculated by Kangsabanik et al., their calculated SLME of $Cs_2Au_2I_6$ for $E \perp c$ at the film thickness of 200 nm is about 75% of the large film thickness limit in contrast to our calculated SLME, which reaches 98% of the large film thickness limit at the film thickness of 200 nm. There is another difference between the results reported by Kangsabanik et al. and those obtained in this work; the SLME of $Cs_2Au_2I_6$ for $E \parallel c$ calculated by Kangsabanik et al. is smaller than that of $MAPbI_3$ at any given film thickness in contrast to the result obtained in this work that the SLME of $Cs_2Au_2I_6$ for $E \parallel c$ is almost equal to that of $MAPbI_3$ at any given film thickness.

4. Conclusions

We have studied the electronic and optical properties of the mixed valence perovskite $Cs_2Au_2X_6$ using the fully relativistic all-electron calculations. The absorption coefficients were calculated within the independent particle approximation combined with a phenomenological approach. In particular, we calculated the optical transition matrix elements using the four-component spinors obtained as the solutions of the Dirac-Kohn-Sham equations. $Cs_2Au_2X_6$ exhibit indirect fundamental band gaps although the differences between the indirect and direct band gaps are small. In the main part of the solar spectrum, the absorption coefficients of $Cs_2Au_2Br_6$ and $Cs_2Au_2I_6$ for $E \perp c$ are larger than that of $MAPbI_3$. The maximum absorption coefficients of $Cs_2Au_2Br_6$ and $Cs_2Au_2I_6$ for $E \perp c$ are almost 20×10^4 cm^{-1} at the photon energy of 2 eV. The absorption coefficient of $Cs_2Au_2I_6$ for $E \parallel c$ is comparable to that of $MAPbI_3$. The SLME of $Cs_2Au_2I_6$ in the limit of large film thickness is almost equal to that for $MAPbI_3$. The SLME of $Cs_2Au_2I_6$ for $E \perp c$ is larger than that of $MAPbI_3$ at any given film thickness and reaches 98% of the large film thickness limit at the film thickness of 200 nm. Also, the SLME of $Cs_2Au_2Br_6$ for $E \perp c$ is larger than that of $MAPbI_3$ for the film thicknesses less than 200 nm. The SLME of $Cs_2Au_2I_6$ for $E \parallel c$ is almost equal to that of $MAPbI_3$ at any given film thickness.

References

1) A. Kojima, K. Teshima, Y. Shirai, and T. Miyasaka, J. Am. Chem. Soc. **131**, 6050 (2009).
2) N. Cai, S.-J. Moon, L. Cevey-Ha, T. Moehl, R. Humphry-Baker, P. Wang, S. M. Zakeeruddin, and M. Gratzel, Nano Lett. **11**, 1452 (2011).
3) M.-Z. Liu, M. B. Johnston, and H. J. Snaith, Nature **501**, 395 (2013).
4) J. H. Noh, S. H. Im, J. H. Heo, T. N. Mandal, and S. I. Seok, Nano Lett. **13**, 1764 (2013).
5) N. J. Jeon, J. H. Noh, W. S. Yang, Y. C. Kim, S. Ryu, J. Seo, and S. I. Seok, Nature **517**, 476 (2015).
6) W. S. Yang, J. H. Noh, N. J. Jeon, Y. C. Kim, S. Ryu, J. Seo, S. I. Seok, Science **348**, 1234 (2015).
7) Y. Kanemitsu and T. Handa, Jpn. J. Appl. Phys. **57**, 090101 (2018).
8) H. Fujiwara, M. Kato, M. Tamakoshi, T. Miyadera, and M. Chikamatsu, Phys. Status Solidi A **215**, 1700730 (2018).
9) T. A. Berhe, W.-N. Su, C.-H. Chen, C.-J. Pan, J.-H. Cheng, H.-M. Chen, M.-C. Tsai, L.-Y. Chen, A. A. Dubale, and B.-J. Hwang, Energy Environ. Sci. **9**, 323 (2016).
10) N. Espinosa, L. Serrano-Luján, A. Urbina, and F. C. Krebs, Sol. Energy Mater. Sol. Cells **137**, 303 (2015).
11) A. Babayigit, D. D. Thanh, A. Ethirajan, J. Manca, M. Muller, H.-G. Boyen, and B. Conings, Sci. Rep. **6**, 18721 (2016).
12) S. F. Hoefler, G. Trimmel, and T. Rath, Monatsh. Chem. **148**, 795 (2017).
13) F. Hao, C. C. Stoumpos, D. H. Cao, R. P. H. Chang, and M. G. Kanatzidis, Nat. Photonics **8**, 489 (2014).
14) N. K. Noel, S. D. Stranks, A. Abate, C. Wehrenfennig, S. Guarnera, A.-A. Haghighirad, A. Sadhanala, G. E. Eperon, S. K. Pathak, M. B. Johnston, A. Petrozza, L. M. Herza, and H. J. Snaith, Energy Environ. Sci. **7**, 3061 (2014).
15) N. Wang, Y. Zhou, M.-G. Ju, H. F. Garces, T. Ding, S. Pang, X. C. Zeng, N. P. Padture, and X. W. Sun, Adv. Energy Mater. **6**, 1601130 (2016).
16) K. P. Marshall, M. Walker, R. I. Walton, R. A. Hatton, Nat. Energy **1**, 16178 (2016).
17) M. R. Filip and F. Giustino, J. Phys. Chem. C **120**, 166 (2016).
18) M.-G. Ju, J. Dai, L. Ma, and X. C. Zeng, J. Am. Chem. Soc. **139**, 8038 (2017).
19) S. Nagane, D. Ghosh, R. L. Z. Hoye, B. Zhao, S. Ahmad, A. B. Walker, M. S. Islam, S. Ogale, and A. Sadhanala, J. Phys. Chem. C **122**, 5940 (2018).

20) G. Giorgi and K. Yamashita, Chem. Lett., **44**, 826 (2015).
21) A. H. Slavney, T. Hu, A. M. Lindenberg, and H. I. Karunadasa, J. Am. Chem. Soc., **138**, 2138 (2016).
22) E. T. McClure, M. R. Ball, W. Windl, and P. M. Woodward, Chem. Mater. **28**, 1348 (2016).
23) G. Volonakis, M. R. Filip, A. A. Haghighirad, N. Sakai, B. Wenger, H. J. Snaith, and F. Giustino, J. Phys. Chem. Lett. **7**, 1254 (2016).
24) M. R. Filip, S. Hillman, A. A. Haghighirad, H. J. Snaith, and F. Giustino, J. Phys. Chem. Lett. **7**, 2579 (2016).
25) G. Volonakis, A. A. Haghighirad, H. J. Snaith, and F. Giustino, J. Phys. Chem. Lett. **8**, 3917 (2017).
26) T. Nakajima and K. Sawada, J. Phys. Chem. Lett. **8**, 4826 (2017).
27) L. Debbichi, S. Lee, H. Cho, A. M. Rappe, K.-H. Hong, M. S. Jang, and H. Kim, Adv. Mater. **30**, 1707001 (2018).
28) G. Giorgi, K. Yamashita, and M. Palummo, J. Mater. Chem. C **6**, 10197 (2018).
29) J. Kangsabanik, S. Ghorui, M. Aslam, and A. Alam, arXiv:1905.09861.
30) N. Matsushita, H. Ahsbahs, S. S. Hafner, and N. Kojima, Rev. High Pressure Sci. Technol. **7**, 329 (1998).
31) W. Denner, H. Schulz, and H. D'Amour, Acta Cryst. A **35**, 360 (1979).
32) S. C. Riggs, M. C. Shapiro, F. Corredor, T. H. Geballe, I. R. Fisher, G. T. McCandless, and J. Y. Chan, J. Cryst. Growth **355**, 13 (2012).
33) N. Matsushita, H. Kitagawa, and N. Kojima, Acta Cryst. **C53**, 663 (1997).
34) X. J. Liu, K. Matsuda, Y. Moritomo, A. Nakamura, and N. Kojima, Phys. Rev. B **59**, 7925 (1999).
35) B. Winkler, C. J. Pickard, M. D. Segall, and V. Milman, Phys. Rev. B **63**, 214103 (2001).
36) K. Momma and F. Izumi, J. Appl. Crystallogr. **44**, 1272 (2011).
37) S. Suzuki and K. Nakao, J. Phys. Soc. Jpn. **66**, 3881 (1997).
38) S. Suzuki and K. Nakao, J. Phys. Soc. Jpn. **68**, 1982 (1999).
39) S. Suzuki and K. Nakao, J. Phys. Soc. Jpn. **69**, 532 (2000).
40) M.-F. Li, T. Ariizumi, and S. Suzuki, J. Phys. Soc. Jpn. **76**, 054702 (2007).
41) S. Suzuki and M. Tsuyama, J. Phys. Soc. Jpn. **88**, 075002 (2019).
42) J. P. Perdew, K. Burke, and M. Ernzerhof, Phys. Rev. Lett. **77**, 3865 (1996).
43) L. Yu and A. Zunger, Phys. Rev. Lett. **108**, 068701 (2012).
44) W. Shockley and H. J. Queisser, J. Appl. Phys. **32**, 510 (1961).

45) “Reference Solar Spectral Irradiance: Air Mass 1.5”, https://rredc.nrel.gov/solar//spectra/am1.5/.
46) L.-K. Hua and Y. Wang, *Applications of Number Theory to Numerical Analysis* (Springer-Verlag, Berlin, 1981).
47) W. Setyawan and S. Curtarolo, Comput. Mater. Sci. **49**, 299 (2010).
48) M. Shirayama, H. Kadowaki, T. Miyadera, T. Sugita, M. Tamakoshi, M. Kato, T. Fujiseki, D. Murata, S. Hara, T. N. Murakami, S. Fujimoto, M. Chikamatsu, and H. Fujiwara, Phys. Rev. Appl. **5**, 014012 (2016).